



Synthesis of Visible Light Response S-SnO₂ Catalyst for Optimized Photodegradation of Bromophenol Blue

Umar Ibrahim Gaya¹ , Kabiru Isya Sani¹ , Abubakar Hamisu^{1,2*} 

¹Department of Pure and Industrial Chemistry, Bayero University Kano, 700241 Knao, P.M.B. 3011, Kano State, Nigeria

²Department of Chemistry, Kano University of Science and Technology Wudil, P.M.B. 3011 Kano, Nigeria

* Corresponding author: Abubakar HAMISU (E-mail: ababakary@gmail.com)

ABSTRACT

In the present study, sulfur-doped tin dioxide (S-SnO₂) catalysts have been synthesized by precipitation of aqueous SnCl₄ in the presence of NH₃. The synthesized catalysts have been characterized by scanning electron microscopy (SEM), Fourier transforms infrared spectrometry (FTIR) energy dispersive x-ray (EDX) and x-ray diffraction (XRD). The photocatalytic performance of the synthesized S-SnO₂ catalysts was optimized for bromophenol blue (BPB) degradation under visible light irradiation based on central composite design (CCD). Input variables adopted for the optimization are catalysts dosage, initial concentration of bromophenol blue and pH. Optimal conditions for the efficient BPB photodegradation were found to involve catalyst dosage of 0.4 g/L, initial BPB concentration of 5 mg/L and pH 8 under which maximum percentage degradation of 92.33% BPB degradation over 0.4g S-SnO₂ was attained for 120 min visible light irradiation. Thus, the 0.4g S-SnO₂ sample prepared under the found optimal dopant amount yielded the maximal removal efficiencies.

ARTICLE INFO

Keywords:

Bromophenol blue
S-SnO₂ Photocatalyst
Visible light

Received: 12-10-2021

Accepted: 15-11-2021

ISSN: 2651-3080

DOI: 10.54565/jphcfum.1008388

1. Introduction

Organic dyes are substances that make water to be polluted. Manufacturing industries that used dyes extensively in textile, dyeing, paper, leather, cosmetics and food processing to make their products attractive and valuable [1]. At the end of the process, these organic dyes are released into the environment as effluents or wastewater pollutants. The release of these waste products in the water stream creates a vacuum in making the water to be polluted. The effluents or wastewater from the industries are characterized by high alkalinity, biological oxygen demand and require proper treatment before they are discharged into the water streams. The presence of color in water prevents sunlight penetration into the water stream and reduces photosynthesis action. Some dyes are reported to cause carcinogenic and mutagenic problems. The presence of a very small concentration of dyes in water makes them unaesthetic and affect human as well as aquatic life and hence need to be treated. Bromophenol blue (BPB) is a good example of industrial dye, it is derived from triphenylmethane, highly water soluble, commonly found in the effluent from the textile and chemical industries. Its high concentration of Bromophenol

Blue (BPB) wastes could reach a maximum of 50mg/l for a period of intense industrial activities [2].

However, the dyes from wastewater are very difficult to treat because of their synthetic origin and complex aromatic structure [3]. To overcome these problems various conventional methods have been pressed into practice, in the decolonization and degradation of dyes in the wastes namely; biological treatment methods, coagulation, filtration, adsorption by activated carbon and reverse osmosis [4]. Low cost method such as adsorption by activated charcoal, among these have been proven to be effective but incomplete because the use of activated carbon adsorption can only change the phase of contaminants without destroying them and then leading to another pollution problem [5]. In the biological treatment process, there are also several drawbacks including the slow reaction rates, the control temperature and disposal of activated sludge [6]. Therefore, more effective treatment processes which can completely degrade all organic and inorganic pollutants are required.

Advanced oxidation processes (AOPs) are one of the most important and widely used methods for wastewater treatment. These methods offer several advantages including the complete mineralization and degradation of organic contaminants. Among them, semiconductor-based photocatalytic degradation could be considered as the most efficient [7]. This particular technique involves the use of semiconductors as a catalyst which acts as the medium of oxidation.

Various metal oxide semiconductors such as SnO_2 , ZnO , WO_3 and TiO_2 have been studied and applied as photocatalysts. Photocatalytic degradation of aniline blue dye using different semiconductors such as SnO_2 , ZnO ZnS was reported [8]. The photocatalytic activity of SnO_2 nanofibers on the degradation of Rhodamin B solution under ultraviolet irradiation was evaluated [9]. Photocatalytic destruction of Naproxen using SnO_2 and direct sunlight was reported [10]. It was found that SnO_2 nanostructures are poorly absorbed by the body and shows no significant toxicity nor acts as a carcinogenic agent [11]. The SnO_2 nanostructures are widely exposed as dye-based solar cells, chemical sensors and anode for batteries [12, 13, 14]. It was reported that SnO_2 has a wide bandgap of 3.6eV [15]. The main problem of semiconductors is the wide bandgap. Therefore, it is important to synthesize narrow band gap semiconductors that absorb longer wavelengths of the visible light spectrum.

Many non-metals such as carbon, nitrogen and Sulphur have been found to improve the efficiency of a photocatalyst which influence the light absorption, photo reactivity and morphology of semiconductor photocatalyst [16]. Nonmetals as dopant affect the electronic structure and also result in the redshift in the adsorption spectra i.e., shifting wavelength from ultraviolet to the visible light region and this improve utilization percentage of visible light [17]. The structure of Bromophenol blue is shown in Fig. 1.

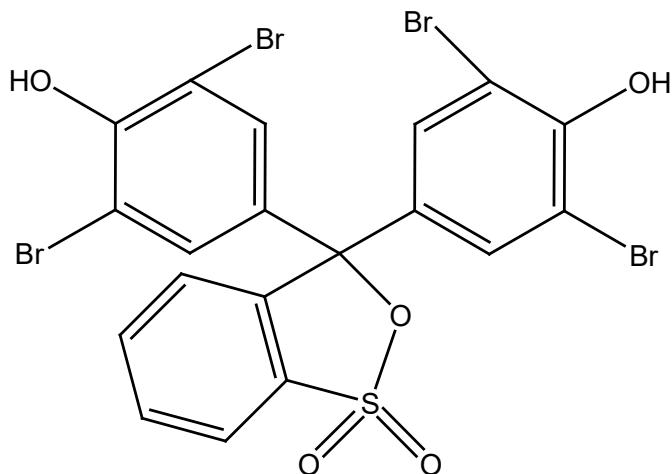


Fig. 1. Structural Formula of Bromophenol blue

2. Experimental

2.1. Materials

All chemicals are analytical grade and were used without further purification. Stannic chloride pentahydrate ($\text{SnCl}_4 \cdot 5\text{H}_2\text{O}$) was purchased from Sinopharm, Hydrochloric (HCl), Sodium hydroxide (NaOH), Bromophenol blue ($\text{C}_{19}\text{H}_{10}\text{Br}_4\text{O}_5\text{S}$) from sigma and Ammonia (NH_3) from Merck. Double distilled water was used as a solvent in all the experimental studies.

2.2 Synthesis of S-SnO₂ Photocatalyst

The S-SnO₂ powders were synthesized using the precipitation method. In a typical procedure, 2 g of stannic chloride and a certain amount of thiourea were mixed in a beaker containing 100 cm³ deionized water. For complete dissolution the mixture was stirred for 3 h and the pH was adjusted to 7 by adding 5 cm³ of 25% ammonia solution. The resulting solution was further stirred for 2 h until white precipitates were formed. The precipitates were separated from the solution by centrifugation and dried at 100 °C for 24 h. Finally, the powdered was calcinated in a furnace at 750 °C for 3 h to obtain S-SnO₂ catalyst. The SnO₂ was synthesized via the same method but without the addition of the thiourea. The sample synthesized with 0.2, 0.3, 0.4, 0.5 and 0.6% S molar ratio versus SnO₂ during the preparation were named as 0.2g S-SnO₂, 0.3 S-SnO₂, 0.4 S-SnO₂, 0.5g S-SnO₂, and 0.6g S-SnO₂ respectively. Moreover, SnO₂ donate sample prepared without the addition of thiourea.

2.3. Characterization of the Photocatalyst

In order to study the crystals properties of the synthesized SnO₂, X-ray diffraction (XRD) was conducted and the peaks patterns were recorded using (XRD X pert) operated at 40kv and 30kv using CuK α radiation source at λ of 1.540 nm, data were collected at $5^\circ \leq 2\theta \leq 70^\circ$. The Morphology of the doped and undoped catalysts was determined by SEM, recorded using (LEICA Stereo, scan-440 interfaced with Phoenix EDX) operated at 15kV. The spectrum of infrared absorption from the samples is obtained using Fourier transform infrared spectrometer (Cary 630 from Agilent Technologies) within the range of 400-4000cm⁻¹. EDX analysis was performed using energy dispersive spectrometer (OxfordXmax 20) for elemental analysis. Perkin Elmer Lambda 35 UV/Vis/NIR spectrophotometer was used for the calculation of band gap energy utilizing Schuster-Kubelka-Munk relations.

2.4. Experimental Design

The experiment was designed with the aid of Response Surface Methodology (RSM) using Central Composite Design (CCD) [18, 19]. The design with three effective variables was run by the design-expert version 6.0.6. The plan includes 8 factor points (2^n), 6 axial points ($2n$), and 3 center points (replications), so that a total number of 17 experiments were performed in a randomized order as required by the design. The adequacy of the proposed model is then revealed using the diagnostic test provided by

analysis of variance (ANOVA). The design factors to be investigated were initial Bromophenol blue concentration, Catalyst dosage and pH, other parameters such as oxygen supply, temperature and light intensity were kept constant. The number of experiments carried out in the design was guided by the formula $N=2^n + 2n + 3$, where N is the number of experiments and n is the number of factors studied. The experimental design was constructed using three different coded values for each variable, i.e., factorial point (-1 and +1 which represent low and high values), axial points (-1.68 and +1.68 which represent maximum and minimum values) and center point which is represented by "0".

2.5 Photocatalytic Degradation of Bromophenol Blue

In the photocatalytic experiment, the required amounts of BPB (5-25mg/L) and the catalyst (0.1-0.5g) was magnetically stirred continuously at 1000rpm for 10mins to attain absorption-desorption prior to irradiation. The pH of the suspension was adjusted using 0.1M NaOH and 0.1M HCl. The solution was irradiated for 120 min using a halogen lamp (0.0129w/m²). Aliquot of 5ml Samples were taken from the reactor through the specialized sample port in

the reactor at a regular time interval of 30min, the withdrawal samples were centrifuge to remove the catalyst if any present in it and the supernatant was monitored in a Perkin Elmer Lambda 25 UV-visible spectrophotometer at 592 nm to determine the concentration of remaining BPB in the solution. Here, in this study, the changes in the UV-vis absorption peak of BPB at 592nm are taken into account and all the experiments were conducted at 33 °C. For comparison of the photocatalytic activity between SnO₂ and S-SnO₂, another two set of experiments using the optimum conditions were conducted. Table 1 shows the actual level of operation variables.

2.6 Direct Photolysis and Adsorption in the Dark

The photolytic decomposition of BPB in the presence of visible light and in the absence of the catalyst was investigated at the optimum condition, for the adsorption study also the decomposition of the BPB was investigated in the presence of S-SnO₂ but in the absence of visible light. The combined experimental results were shown in Fig: 4(d)

Table 1 Actual Values of Coded Level of the Operating Variables

Factors	Codes and Levels				
	-1.68	-1	0	+1	+1.68
BPB concentration (mg/L) [A]	5	10	15	20	25
Catalysts dosage (g/L) [B]	0.2	0.3	0.4	0.5	0.6
pH [C]	3	6	8	11	13

3. Results and Discussion

3.1. The XRD Studies

Fig. 2 a and b show the XRD patterns of pure SnO₂ and S-SnO₂ synthesized by precipitation method operated at 40kv and 30kv using CuK α radiation source at λ of 1.540 Å, data were collected at $5^\circ \leq 2\theta \leq 70^\circ$ and the values was compared with (JCPD card No. 41-1445) with 2θ value of 26.51^o which are further supported with a strong peak at 26.45 with intensity of 28.86 for both SnO₂ and S-SnO₂ catalysts. Peaks were observed at 33.74, 34.97 and 53.61 confirming the presence of the tetragonal structure of both S-SnO₂ and SnO₂ catalysts. It implies that all diffraction peaks were well assigned to a tetragonal crystalline phase of SnO₂ and the doping does not change the tetragonal rutile structure of SnO₂. The lattice parameter (a, b and c) of the S-SnO₂ and SnO₂ photocatalysts was given from the XRD report. The

rutile phase was compared to the lattice cell parameters for the rutile phase reported by JCPD. The value calculated considering (110) and (101) lattice plane for the rutile corresponding 2θ values of 28.86 and 33.74 where $a=b=0.398\text{nm}$ and $c=0.322\text{nm}$. The lattice parameters for the tetragonal rutile structure calculated for the (101) and (200) lattice with corresponding 2θ value of 26.45 and 34.97 was also in good agreement with the reported value of $a=b=0.4751\text{nm}$ and $c=0.3197\text{nm}$. The values obtained from the diffraction data of synthesized both doped and undoped catalysts were $a=b=0.4751\text{nm}$ and $c=0.3197\text{nm}$. The average crystallite size (d) of the sample was determined from the X-ray broadening line using Debye-Scherrer equation [21]:

$$D = \frac{k\lambda}{\beta \cos\theta} \quad (1)$$

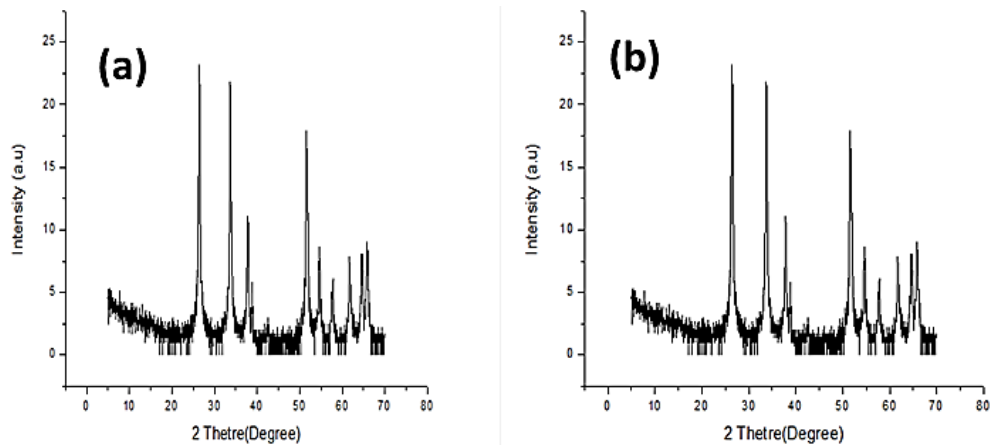


Fig. 2. The XRD peaks of (a) bare SnO₂ and (b) S-SnO₂

3.2. Band Gap Analysis

Schuster-Kubelka-Munk's relation was utilized to calculate the band gap energy from absorption data in order to determine the wavelength of light necessary for the excitation of S-SnO₂ photocatalyst. The bandgap energy of

the bare SnO₂ photocatalyst was found to be 3.66 eV (Fig. 3a) and a redshift is readily observed when it was doped with sulfur (S-SnO₂) which was reduced to 3.35 (Fig. 3b) which shows that more of the visible light can now be absorbed by the doped photocatalyst.

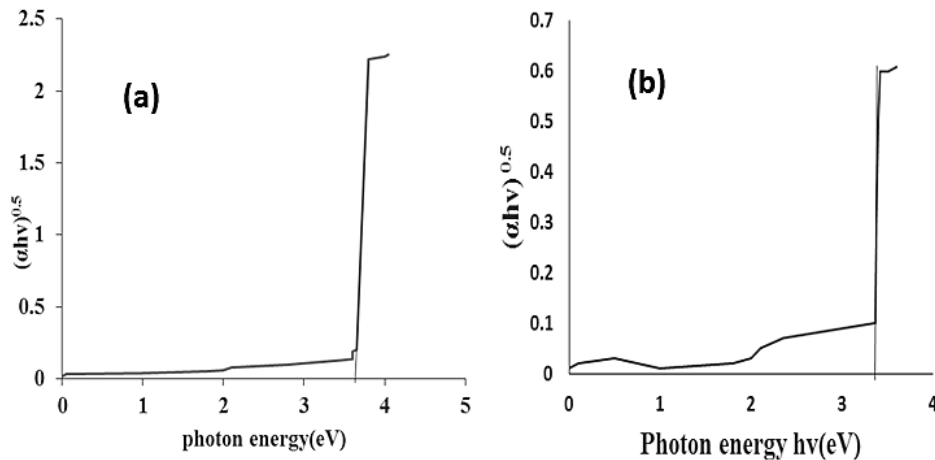


Fig. 3. Tauc's plot for (a) bare SnO₂ and (b) S-SnO₂

3.3. FTIR Analysis

The FTIR spectra of prepared SnO₂ and S-SnO₂ photocatalysts are shown in Fig. 4 a and b. The FTIR spectra show several bands. The band of absorption peak at 579cm⁻¹

and 1126cm⁻¹ is attributable to Sn-O and C-N respectively. The absorption peak at 1626cm⁻¹ indicates the presence of Sn-O-Sn [20]. The absorption peak at 722cm⁻¹ is due to S-N vibration.

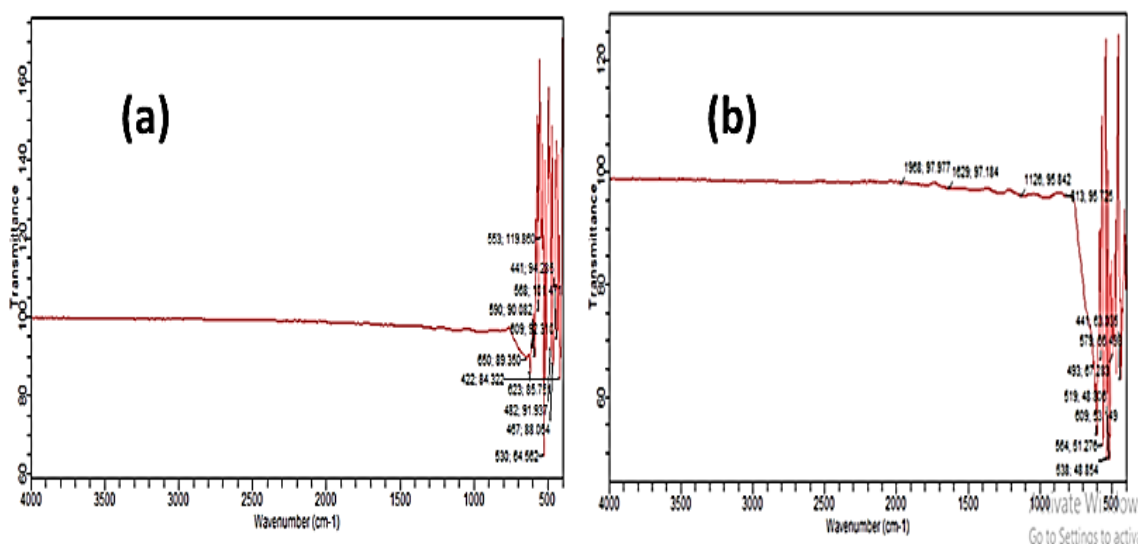


Fig. 4. The FTIR spectra of (a) SnO₂ and (b) S-SnO₂

3.4. The SEM Analysis

The SEM images of the SnO₂ and S-SnO₂ photocatalysts are depicted in Fig. 5. It can be seen from the figure, the surface of S-SnO₂ particles do not differ significantly from those the pure SnO₂ in which both are rough. However, S-SnO₂ is less

agglomerated in comparison to bare SnO₂ and this can be attributed due to the present sulfur dopant that may prevent aggregation of the particles. Estimated grain sizes from the figures reveal that the sulfur doped photocatalyst may have a smaller particle size than the bare SnO₂ photocatalyst.

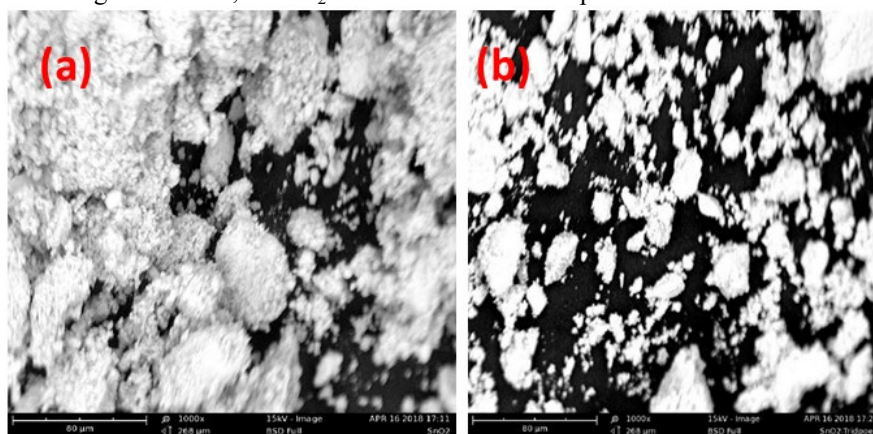


Fig. 5. (a) SEM image of (a) SnO₂ and (b) S-SnO₂

3.5. The EDX Analysis

From the EDX spectrum, the chemical composition of SnO₂ and S-SnO₂ can be examined. The EDX spectrum represented in Fig. 4 and Table 2, Fig. 4 (a) show strong signals in Sn and O regions. The signal approximately at around 3.6, 3.9 and 4.4KeV is due to the presence of Sn, peak at 0.5keV indicate the presence of O. Other elements are present and are impurities, in Table 2, the sample contains 59.76% Sn, 23.81% O, hence the sample synthesized is 87.57% SnO₂. The chemical composition of S-SnO₂ can be examined from the EDX spectrums 5 in Fig. 4 and Table 2. Which shows the percentage composition of the individual elements present. The EDX spectrum shows strong signals in the Sn, and O regions, at low regions also a

signal of S is observed. The signal approximately at around 3.4, 3.8 and 4.4keV is due to the presence of Sn. The signal observed at 2.4keV in spectrum 5 is due to the presence of Sulphur. This was further supported by 0.09% atomic weight of Sulphur in Table 2. This clearly indicates the introduction of Sulphur in the structure of the SnO₂ after addition of thiourea in the preparation process. However, there are some other weak signals that are observed at around 0.9, 8.0, and 8.9keV due to the presence of Cu, 2.2keV and 9.7keV is due to the presence of Au. The signal at around 0.4keV signal is due to the presence of N these are impurities, the presence of these impurities appeared during operation, hence the presence of these impurities can be neglected. Therefore, the signals observed confirmed the formation of S-SnO₂ in spectrum 5.

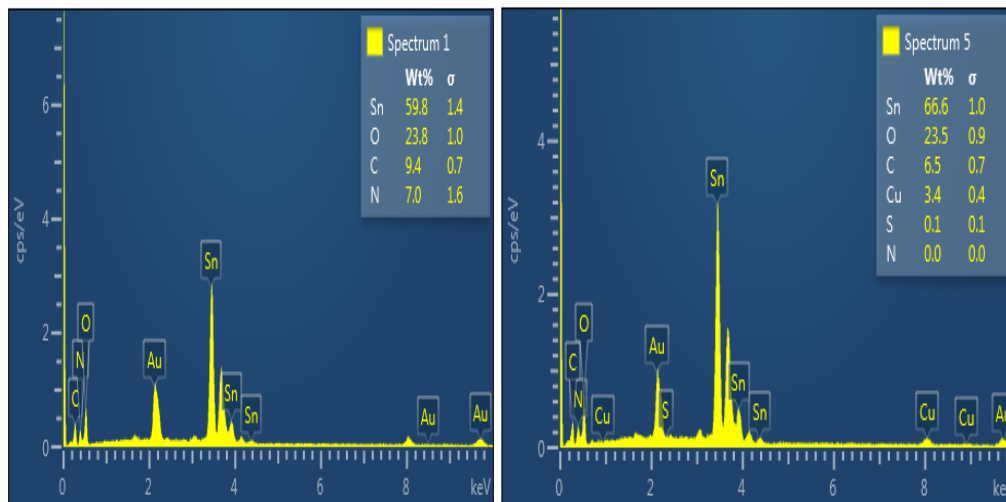


Fig. 6. The EDX spectrum of synthesized of (a) SnO₂ and (b) S-SnO₂ photocatalyst

Table 2. Elemental compositions of the SnO₂ and S SnO₂ from EDX spectrum

S-SnO ₂	weight%	SnO ₂	weight%
C K	6.47	C K	9.43
N K	0.00	N K	7.00
O K	23.49	O K	23.81
S K	0.09		
Cu K	3.38		
Sn K	49.88	Sn	59.76

Table 3. Properties of synthesized catalysts

Catalysts	Particle Size (nm)	Surface Area (m ²)	Unit cell Volume (Å ³)	Density (kg/m ³)	Specific Surface (m ² /kg)
SnO ₂	27.33	3x10 ⁻⁷	72.15	6936	5.99x10 ¹⁷
S-SnO ₂	32.63	3.34 x10 ⁻¹⁵	72.15	6936	6.67x10 ⁹

3.6. Photocatalytic Experiment

To determine the photocatalytic activity of the synthesized S-SnO₂ photocatalyst, the change in optical absorption at 598 nm of BPB solutions are recorded during the photodegradation process. To obtain relevant information about the photocatalytic performance, it is necessary to perform experiments from which any possible direct photolysis or adsorption of material on the photocatalyst was excluded. In this regard, experiments were made (i) under UV irradiation without TiO₂ photocatalyst (photolysis) and (ii) in dark with TiO₂ photocatalyst (adsorption). The results showed that in both cases, no significant disappearance of

BPB was observed (Fig. 7c). The BPB removal observed comes predominantly from photocatalytic degradation by TiO₂ photocatalyst, indicating that the system is working in a pure photocatalytic regime.

3.6.1. Effect of Initial BPB Concentration

The initial dye concentration of the pollutant is one of the most important parameters in the photocatalytic process. It was found that the decomposition or degradation of pollutant increase with substrate concentration. The effect of substrate concentration on the photocatalytic degradation of Bromophenol blue was studied at different concentration

(ranging from 5mg/L-25mg/L) and the result is depicted in Fig. 7a. There is a decrease in the %degradation of the Bromophenol blue dye as the initial concentration increases from 5mg/L-25mg/L at fixed pH and catalyst dosage. This decrease in photodegradation is due to the obstruction of light penetration into the solution, as the path length of photons entering the solution decreases with an increase in concentration [22]. Further, the higher the initial concentration of BPB, the greater catalyst surface area is required for degradation of BPB. This also leads to additional catalyst loading which ultimately results in increasing opacity of the solution [23]. Therefore, the minimal optimum concentration of BPB solution is required for better photodegradation efficiency.

3.6.2. Effect of Catalyst Loading

The effect of the amount of S-SnO₂ catalyst on degradation or decomposition of Bromophenol blue was studied in the range of (0.2-0.6g) and the result was reported in Fig. 7b. Initial concentration of 5mg/L of the pollutant and pH 8

was used to study the effect of catalyst loading. Initially, there was an increase in the rate of degradation or decomposition of Bromophenol blue as the amount of catalyst increased. The degradation rate reached 0.4g as the optimum value. A similar result was reported by [24] to evaluate the photocatalytic activities of methyl green and formaldehyde using SnO₂ composite films. The increase in the degradation or decomposition efficiency with an increase in catalyst dosage can be explained by the increase in the number of active surfaces for desorption [25]. With an increase in catalyst dosage, the total active surface area for light absorption increases, thereby increasing the number of hydroxyl and/ superoxide radicals. Furthermore, the decrease of photocatalytic degradation efficiency observed at amount beyond optimum catalyst loading may be attributable to factors aggregation of catalyst particle at high an amount causing a decrease in number of surface-active sites and an increase in opacity and light scattering of S-SnO₂ particles at high catalyst loading leading to decrease in the passage of irradiation through the sample.

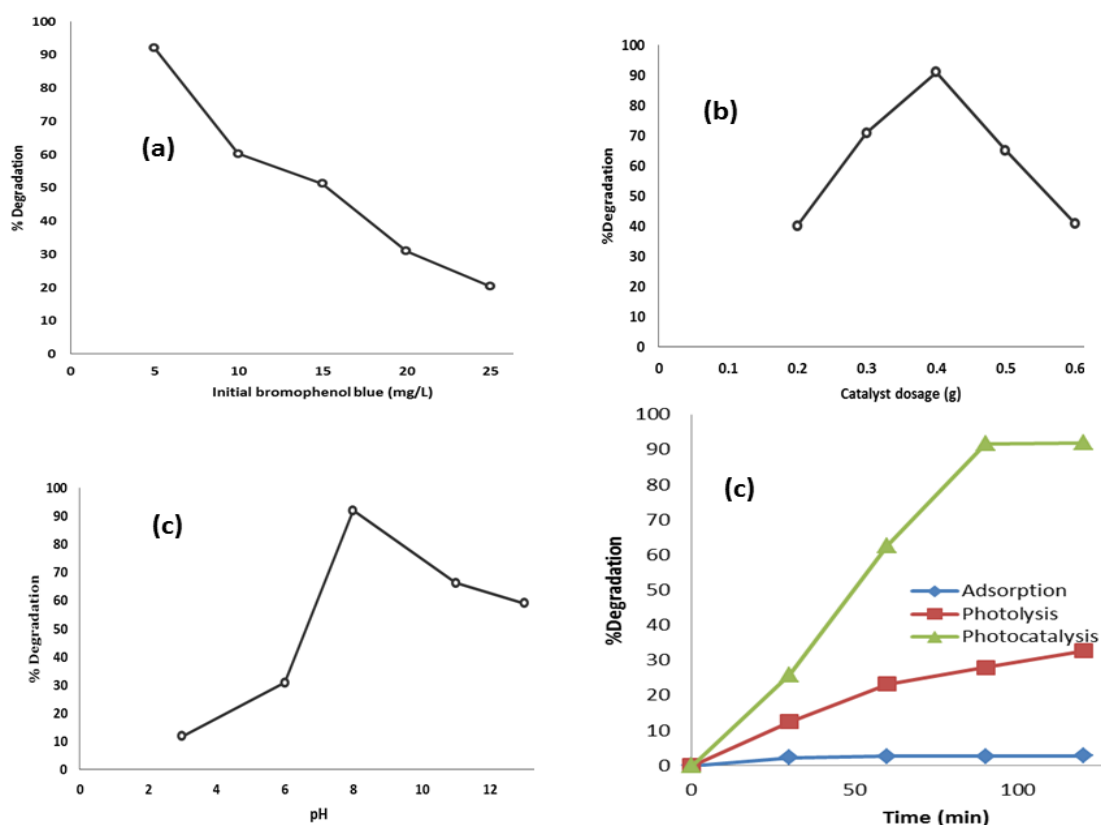


Fig. 7. Effects of (a) initial con (mg/L), (b) catalyst dosage (g), (c) pH, and (d) adsorption, photolysis and photocatalysis studies on degradation of BPB

3.6.3. Effect of pH

The pH is another important parameter in the photocatalytic process [26], it indicates the charge properties of the photocatalyst and the size of the aggregates it forms, Bromophenol blue is basic in nature. The influence of pH on

the photodegradation of the Bromophenol blue was shown in Fig. 7 c. The amplitude of the pH was from 3 to 13. It was found that the degradation increases from 3 to 8, and decreases from value above 8 to 13, the optimum pH recorded was 8, with 91.91% degradation efficiency. The pH dependence was in agreement with the study of degradation

of Bromophenol blue by [27]. But the optimum pH recorded in their study was found to be (pH= 6.65) this discrepancy is

3.6.4. Response Surface Methodology (RSM)

The degradation efficiency values obtained from the experiment (% D) were processed using RSM to obtain statistically valid predicted values. A quadratic polynomial model was used to develop the mathematical relationship between the response and the independent process variables. The empirical relationships between the responses (%D) and independent variables are presented by Eq. (2).

$$\begin{aligned} \%D = & 50.41 - 16.69[A] + 2.86[B] + 10.87[C] + \\ & 2.27[A][A] - 3.25[B][B] - 5.04[C][C] + \\ & 0.10[A][B] - 2.05[A][C] + \\ & 1.65[B][C] \end{aligned} \quad (2)$$

Each coefficient of the variable in the equation estimates the change in mean response per unit increase in the associated independent variable when the other variable is held constant. The degradation efficiency (%D) obtained by photocatalytic degradation process of MB has been predicted by Eq. (2) and the obtained results are presented in Table 4. It can be seen from the tables that, there is a good correlation between the experimental and predicted %degradation as testified by linear normal plot of residuals (Fig. 8). Majority

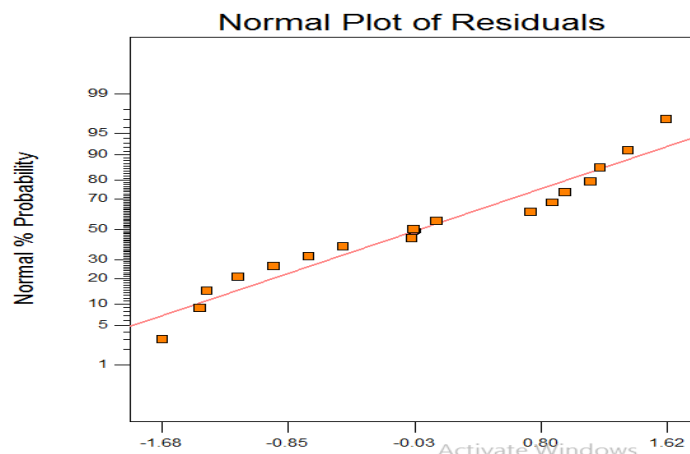
attributable to the nature of the catalyst used which are different for the study.

of the points on the normal probability plot lie roughly on a straight line, so it can be concluded that the estimated effects are the real and differ markedly from noise.

The ANOVA analysis is the integral part of the data analysis and is the more reliable way to evaluate the quality of the model fitted [28]. The statistical significance of the CCD model was assessed by ANOVA. Table 5 shows the analysis of variance for BPB degradation efficiency. The results revealed that the obtained models can be successfully used to navigate the design space. Value of Prob > F less than 0.0500 imply that the model terms are significant while values greater than 0.1000 are demonstrated as insignificant for the regression model. In this study of BPB degradation F Value of 10.29 implies the model is significant. The goodness of the Fit of the model is also checked by R^2 value, the value of the R^2 was found to be 0.9297 which implies that this model is statistically significant. Moreover, "Adeq precision" is used to determine the signal to noise (S/N) ratio to determine the validity of the model. A ratio greater than 4 is recommended. In this case, the study of the degradation of the BPB "adeq precision of 11.281 was obtained which indicate an adequate signal. It also shows that this model can be used to navigate the design space. The "Lack of Fit F-value" of 253.13 implies the Lack of Fit is significant. There is only a 0.39% chance that a "Lack of Fit F-value" this large could occur due to noise.

Table 4. Central composite design matrix and the value of response

Run after 120 min.	Actual (coded) Variables			%Degradation	
	A	B	C	Actual	Predicted
1	15(0)	0.4(0)	8(0)	50.40	50.20
2	20(+1)	0.5(+1)	6(-1)	14.47	20.20
3	20(+1)	0.3(-1)	11(+1)	37.67	42.11
4	10(-1)	0.3(-1)	11(+1)	75.71	70.88
5	5(-1.68)	0.4(0)	8(0)	84.91	91.91
6	10(-1)	0.4(0)	8(0)	50.41	51.20
7	20(+1)	0.3(-1)	6(-10)	23.30	30.88
8	15(0)	0.4(0)	8(0)	50.41	50.11
9	15(0)	0.2(-1.68)	8(0)	46.03	40.00
10	15(0)	0.4(0)	13(+1.68)	54.45	60.20
11	20(+1)	0.5(+1)	11(+1)	35.43	33.11
12	10(-1)	0.5(+1)	11(+1)	72.71	66.23
13	10(-1)	0.5(+1)	6(-1)	43.55	40.18
14	25(+1.68)	0.4(0)	8(0)	28.78	20.20
15	15(0)	0.4(0)	3(-1.68)	17.88	10.57
16	15(0)	0.6(+1.68)	8(0)	36.41	40.88
17	10(-1)	0.3(-1)	6(-1)	52.78	52.20

**Fig. 8.** Normal probability plots

Source	Sum square	o DF	Mean square	F value	Prob>F	Remarks
Model	6137.11	9	681.90	10.29	0.0028	significant
A	3804.36	1	3804.36	57.39	0.0001	
B	111.66	1	111.66	1.68	0.2355	
C	1615.12	1	1615.12	24.37	0.0017	
A ²	58.28	1	58.28	0.88	0.3796	
B ²	119.11	1	119.11	1.80	0.2220	
C ²	286.11	1	286.11	4.32	0.0764	
AB	0.082	1	0.082	1.237E-003	0.9729	
AC	33.66	1	33.66	0.51	0.4991	
BC	21.88	1	21.88	0.33	0.5836	
Residual	464.01	7	66.29			
Lack of Fit	463.28	5	92.66	253.13	0.0039	significant

Table 5. ANOVA for response surface quadratic model

The effect of the operating variables is presented by the 3D response surfaces in Fig. 9. It can be seen from Fig. 9a, the degradation efficiency increases with an increase in the catalyst dosage towards the intermediate (up to 0.4g/L) and decrease with further addition of the catalyst. However, the degradation efficiency increases with a decreasing initial

concentration of bromophenol blue. The same observation was made in the case of interplay of catalyst dosage and pH (Fig. 9b). In the case of pH and bromophenol blue initial concentration (Fig. 9c), the degradation efficiency decreased as the amount of these variables increased.

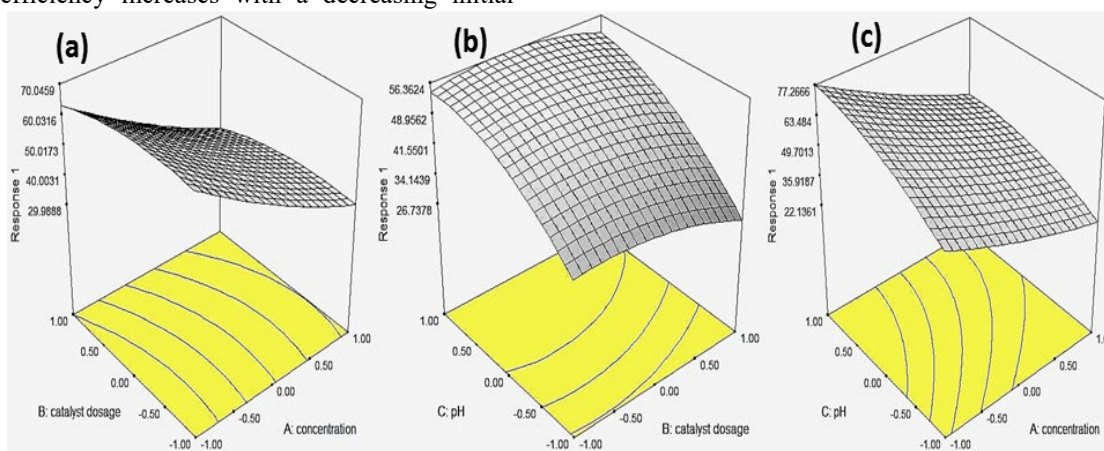


Fig. 9. The 3D response surface of BPB dye degradation efficiency as a function of (a) catalyst dosage and BPB initial concentration (b) pH and catalyst dosage and (c) pH and PBP initial concentration

3.6.5. Comparative Photocatalytic Activity

Table 6 showed the photocatalytic degradation of the synthesized bare SnO₂ and S-SnO₂ photocatalysts under UV irradiation for 120 min. It can be seen, the catalytic performance of bare SnO₂ was found to be 50.2% which significantly increased to 92.33% for sulfur doped photocatalyst (S-SnO₂). The results revealed that, the

catalyst may exhibit better photocatalytic degradation efficiency due to the two fact or factors [10]: Firstly, the introduction S result in the formation of smaller particle size and thus provide a large surface area on the catalyst. Thus, more active sites will be available which lead to the increase in the adsorption of O₂ and H₂O, and hence increase the generation of radicals [29]. Secondly, S may lead to the adsorption of BPB molecule to which the availability of the

BPB molecule on the surface of the photocatalyst is more and thereby results in faster and better photodegradation

efficiency [30, 31].

Table 6 Comparative Photocatalytic Activity Results

Catalysts	A	B	C	%Degradation
SnO ₂	5(-1.68)	0.4(0)	8(0)	50.20
S-SnO ₂	5(-1.68)	0.4(0)	8(0)	92.33

4. Conclusion

SnO₂ and S-SnO₂ photocatalysts synthesized by precipitation method followed by photodegradation of Bromophenol using visible light as a driven agent show a very good photocatalytic activity. In about 120 minutes at the optimum conditions, 91.91% of Bromophenol blue has been found to degrade using S-SnO₂. However, using SnO₂ photocatalyst at the same conditions only 50.20% have been found to be degraded, hence the doped catalyst performed better in the degradation of Bromophenol blue than undoped catalyst under the same conditions. Furthermore, the bandgap was successfully turned and reduced to 3.37eV which is very close to the bandgap energy of bulk SnO₂. This reduced

bandgap energy makes the synthesized S-SnO₂ a brilliant photocatalyst under visible light. The result of photolysis, photocatalysis and adsorption study shows that light has an influence on the photocatalytic degradation of the BPB.

Acknowledgement

The authors acknowledge the Jigawa State College of Education Gumel for their support.

References

- [1] T. Robinson, G. McMullan, Marchant R. and P. Nigam, Remediation of Dyes in Textile Effluent: A Critical Review on Current Treatment Technologies with a Proposed Alternative, *Bioresource Technology*, 2001, 77, 247-255.
- [2] F. Alinsafi, E.M. Evenou, M.N. Abdulkarim, O. Pons, A. Zahra, A. Benhammou, N.A. Yacoubi, Treatment of Textile Industries Wastewater by Supported Photocatalysis, *Dyes and Pigment*, 2007, 74, 439-445.
- [3] S. Asha, and V. Thiruvengkatachari, Decolorization of Dye Wastewaters by Bioabsorbents A Review, *Journal of Environmental Management*, 2010, 91, 1915-1929.
- [4] D. Beydoun, R. Amal, G. Low and S. McEvoy, Role of Nanoparticles in Photocatalysis, *Journal of nanoparticle Research*, 1999, 1, 432-458.
- [5] E. Kusvuran, and E. Oktay, Degradation of Aldrin in Adsorbed System using Advanced Oxidation Process: Comparison of Treatment Methods, *Journal of Hazardous Materials*, 2005, 6, 115-125
- [6] E.A. Kusvuran, O. Samil, A. Malik and E. Oktay, Photocatalytic Degradation Kinetics of di- and tri-Substituted Phenolic Compounds in Aqueous Solution by TiO₂/UV, *Applied catalysis B: Environmental*, 2004, 58, 3-4
- [7] D. Ohtami, Photocatalysis A-Z-What we know and what we do not know in Scientific Sense, *Journal of Photochemistry and photobiology C: Photochemistry Reviews*, 2010, 11, 157-178.
- [8] H.K. Egzar, M.S. Mashkour and A.M. Jude, Study the Photodegradation of Analine Blue in Aqueous Phase by Using Different Photocatalysts, *Asian transaction on basic and applied science*. 2013, 3, 2221-4291.
- [9] L. Chenga, L. Dan, D. Xiangting, M. Qianli, Y. Wensheng, W. Xinlu, Y Hui., J W. inxian and L. Guixia, Synthesis, Characterization and Photocatalytic Performance

of SnS Nanofibers and SnSe Nanofibers Derived from the Electrospinning-made SnO₂ Nanofibers, *Materials Research*, 2017, 20, 1748-1755.

- [10] B. Shamima and M. Ahmaruzzaman, Biogenic Synthesis of SnO₂/activated Carbon Nanocomposite and Its Application as Photocatalyst in the Degradation of Naprozen, *Journal of applied surface science. Journal*, 2018, 449, 780-789
- [11] S. Begum, T.B. Devi and M. Ahmaruzzaman, L-lysine Monohydrate Mediated Facile and Environmental friendly synthesis of SnO₂ Oxide Nanoparticles and there Prospective Applications as a Catalyst for the Reduction and Photo Degradation of Aromatic Compounds, *Journal of environmental chemistry engineering*, 2016, 4, 2976-2989.
- [12] G.J. Shang, M. Wu, J. Huang, Z. Lin. Y. H. Lan, and L. Fan, Facile Synthesis of Mesoporous Tin oxide Spheres and their Applications in Dyes-synthesized Solar Cells, *Journal of physical chemistry C*, 2012, 116, 20140-20145.
- [13] S. Phadunghitidhada, S. Thanasanvorakun, P. Mangkorntong, S. Choopun, N. Mangkorntong and D. Wongratanaphisan, SnO₂ Nanowires Mixed Nanodendrites for High Ethanol Sensors Response, *Current applied physics*, 2011, 11, 1368-1373.
- [14] L. Feng, Z. Xuan, S. Ji, W. Min, H. Zhao and H. Ghao, Preparation of SnO₂ and Performance as Lithium ion Battery Anode, *International journal of electrochemical science*, 2015, 10, 2370-2376.
- [15] C. Dhanya, S. Lakshmi, S.B., Nair, B.K Rajendra and M. Deepa, Band Gap Narrowing and Photocatalytic Studies of Nd³⁺ ion-doped SnO₂ Nanoparticles using Solar Energy, *Bullet Material Science*, 2016, 39, 27-33.

- [16] G. Liu, P. Niu, S.C. Sun, Z. Smith, G.Q. Chen, L. Max, and H.M. Cheng, Unique Electronic Structure Induced High Photoreactivity of Sulfur-doped Graphitic C_3N_4 , *Journal of American Chemical Society*, 2010, 132, 11642-11648.
- [17] Z. Yang, I. Lv, Y. Dai, Z. Xv, and D. Qian, Synthesis of ZnO-SnO₂ Composite Oxide by CTAB Assisted Co-precipitation and Photocatalytic Properties, *Applied Surface Science*, 2010, 256, 2898-2902.
- [18] R.G. Brereton, Applied Chemometrics for Scientists, *John Wiley and Sons*, 2007.
- [19] R.L. Mason, R.F. Gunst, J.L. Hess, Statistical Design and Analysis of Experiments, *John Wiley and Sons*, 2003
- [20] A. Nouri, A. Fokhri and N. Arezu, Synthesis of SnO₂ and C,N,S-tridoped SnO₂ Nanoparticles by Precipitation Method, *Journal of Physical and Theoretical Chemistry*, 2013, 10, 137-142.
- [21] B. D. Cullity, Elements of X-ray diffraction, *Massachusetts: Addison-Wesley*, 2nd ed. 1978
- [22] I. Georgaki, E. Vasilaki, N. Katsarakis, A study on the degradation of carbamazepine and ibuprofen by TiO₂ & ZnO photocatalysis upon UV/visible-light irradiation, *American Journal of Analytical Chemistry*, 2014, 5, 518-534.
- [23] A. Houas, H. Lachheb, M. Ksibi, E. Elaloui, C. Guillard, J. Herrmann, Photocatalytic degradation pathway of Methylene blue in water, *Applied Catalysis B: Environmental*, 2001, 31, 145-157.
- [24] H. Ke, P. Xue-Lei, L. Fang and Y. Ming-Ming, SnO₂ Composite Films for Enhanced Photocatalytic Activities. *Catalysts* 2018, 8, 453.
- [25] U.I. Gaya, A. Abdul Halim, Z. Zulkarnain and Z.H. Mohd, Photocatalytic Degradation of 2, 4-dichlorophenol in Irradiated Aqueous ZnO Suspension, *International Journal of Chemistry*, 2010, 2, 1.
- [26] K. Azad, and P. Gajanan, A Review on Factors Affecting the Photocatalytic Degradation of Hazardous Materials, *International Journal of Material Science and Engineering*, 2017, 1, 18
- [27] A. Ahmed, H.F. Abdel-Khaleh, F.K. Nassar, S.M. Abdel-Ghawad, and A. Seham, Photocatalytic Degradation of Bromophenol Blue in Wastewater Using Pure ZnO and Ag⁺ Doped ZnO, *Quantum Matter*, 2016, 5, 297-304.
- [28] M.A. Bezerra, R.E. Santelli, E.P. Oliveira, L.S. Villar, and L.A. Escalera, Response Surface Methodology (RSM) as a Tool for Optimization in Analytical Chemistry, *Talanta*, 2008, 76, 965-977
- [29] X. Chen and Z. Wu, Effect of different activated carbon as carrier on the photocatalytic activity of Ag-N-ZnO photocatalyst for methyl orange degradation under visible light irradiation, *Nanomaterials*, 2017, 7, 258.
- [30] B. Xing, C. Shi, C. Zhang, G. Yi, L. Chen, H. Guo, and J. Cao, Preparation of TiO₂/activated carbon Composites for photocatalytic degradation of RhB under UV light irradiation, *Journal of Nanomaterials*, 2016, 1-10.
- [31] X.J. Wang, J.K. Song, J.Y. Huang, J. Zhang, X. Wang, R.R. Ma, Wang and J.F. Zhao, Activated carbon-Based magnetic TiO₂ photocatalyst co-doped with iodine and nitrogen for organic pollution degradation, *Applied Surface Science*, 2016, 390, 190-201.